Magnon-Magnon Interaction Induced by Nonlinear Spin-Wave Dynamics

Arfini, Matteo; Bermejillo-Seco, Alvaro; Bondarenko, Artem; Potts, Clinton A.; Blanter, Yaroslav M.; van der Zant, Herre S.J.; Steele, Gary A.

DOI
10.1103/jnpb-2mxx

Publication date
2025

Document Version
Final published version

Published in
Physical review letters

Citation (APA)
Arfini, M., Bermejillo-Seco, A., Bondarenko, A., Potts, C. A., Blanter, Y. M., van der Zant, H. S. J., & Steele, G. A. (2025). Magnon-Magnon Interaction Induced by Nonlinear Spin-Wave Dynamics. *Physical review letters*, *135*(16), 166703. Article 166703. https://doi.org/10.1103/jnpb-2mxx

Magnon-Magnon Interaction Induced by Nonlinear Spin-Wave Dynamics

Matteo Arfini,[1,*,†] Alvaro Bermejillo-Seco,[1,*,‡] Artem Bondarenko,[1] Clinton A. Potts,[2,3] Yaroslav M. Blanter,[1] Herre S. J. van der Zant,[1] and Gary A. Steele[1,§]

[1]*Kavli Institute of Nanoscience, Delft University of Technology, Lorentzweg 1, 2628 CJ Delft, Netherlands*

[2]*Niels Bohr Institute, University of Copenhagen, Blegdamsvej 17, 2100 Copenhagen, Denmark*

[3]*NNF Quantum Computing Programme, Niels Bohr Institute, University of Copenhagen, Copenhagen, Denmark*

(Received 16 June 2025; revised 10 September 2025; accepted 23 September 2025; published 15 October 2025)

We experimentally and theoretically demonstrate that nonlinear spin-wave dynamics can induce an effective resonant interaction between nonresonant magnon modes in a yttrium iron garnet disk. Under strong pumping near the ferromagnetic resonance mode, we observe a spectral splitting that emerges with increasing drive amplitude. This phenomenon is well captured by a theoretical framework based on the linearization of a magnon three-wave mixing Hamiltonian, which at high power leads to parametric Suhl instabilities. The access and control of nonlinear magnon-parametric processes enable the development of experimental platforms in an unexplored parameter regime for both classical and quantum computation protocols.

DOI: 10.1103/jnpb-2mxx

Ferromagnetic resonance (FMR) [1,2] is a well-established experimental technique for studying the dynamics of magnons, collective spin excitations in magnetically ordered materials. The power absorption that arises when the Larmor precession of spins under an external bias field resonates with microwave signals stands at the core of magnonics [3]. Coherent interactions between spin-waves and microwave fields have potential applications in sensing, transduction, and information processing [4–11]. The collective nature of magnons makes them well suited for coupling to photons [12,13], phonons [14,15], and electronic charge [16]. Moreover, their integration with superconducting qubits has enabled the generation of magnon quantum states [7,10,17], while their tunability opens pathways to exploring non-Hermitian band theory [18]. Theoretically, proposals exist for realizing robust magnon squeezed states [19,20] and generating quantum entanglement [21–23].

Most FMR experiments operate in the linear regime, where higher-order processes are negligible. However, at higher magnon amplitudes, nonlinear phenomena such as Suhl instabilities can emerge [24]. These intrinsic nonlinearities stem from higher-order contributions to the magnetic energy density in the Landau-Lifshitz-Gilbert equation [25] and the power expansion of the spin Hamiltonian in bosonic operators under the Holstein-Primakoff transformation [26,27]. The first nonlinear term, which causes the first-order Suhl instability, involves the coupling of three magnon modes in the form of three-wave mixing. Figure 1(a) schematically depicts this coupling for the case of the decay of a zero-momentum mode $\hat{m}_0$ at frequency ω_0 into two counterpropagating modes $\hat{m}_{\pm k}$ at half the frequency $\omega_0/2$. Indirect evidence of these three-magnon interactions has been observed in studies of FMR mode saturation and decay mechanisms [28,29] and, more recently, in cavity magnonics [30] and nanoscale ferromagnets [31–33]. However, a systematic framework for controlling and manipulating the magnon three-wave mixing Hamiltonian has yet to be established, hindering deeper exploration and practical applications of these interactions.

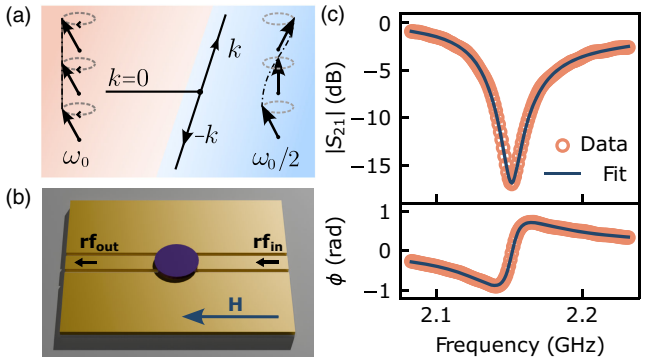

FIG. 1. FMR in a driven YIG disk leading to parametric instability. (a) Three-wave mixing: $k = 0$ mode decays into counter-propagating magnons $\pm k$ at $\omega_0/2$. (b) Device: YIG disk on a 50 Ohm transmission line. (c) Measured FMR amplitude and phase response of the $k = 0$ magnon mode at 28 mT. Solid lines represent a fit yielding $\omega_0/2\pi = 2.15$ GHz and $\gamma_0/2\pi = 58.94$ MHz.

*These authors contributed equally to this work.
†Contact author: m.arfini@tudelft.nl
‡Contact author: a.bermejilloseco@tudelft.nl
§Contact author: g.steele@tudelft.nl

In this Letter, we study a magnon-magnon coupling phenomenon originating from the three-wave interaction in a driven ferrimagnetic disk. Analytical solutions of the Hamiltonian dynamics show that linearizing the magnon three-wave mixing term yields an effective resonant beam-splitter interaction between the mode at $k = 0$ and the excited magnon pair at $\pm k$ [see Fig. 1(a)]. The strength of this coupling shows a nonlinear dependence on the input microwave power. In addition, we show that this effect is visible only below a threshold external magnetic field, above which energy-momentum conservation cannot be satisfied.

The device is a 350-μm-thick, two-sided polished yttrium iron garnet (YIG) ($Y_3Fe_5O_{12}$) disk with a diameter of 5 mm grown along the [111] crystallographic axis by the floating zone method, with a Curie temperature of 559 K [34]. The disk is placed on a 50 Ω transmission line narrower than the magnetic sample, as shown in Fig. 1(b). An external magnetic field H_{ext} is applied parallel to the feedline. We measure the microwave transmission spectrum S_{21} through the transmission line at room temperature using a vector network analyzer as a function of frequency $\omega/2\pi$, microwave power P, and magnetic field. With a single-tone measurement, sweeping the probe in frequency as a function of external field, we observe several magnetostatic modes of the disk. The resonances correspond to Walker modes with azimuthal nodes along the direction of the field [35–37]. Here, we address the most prominent resonance dip in the spectrum corresponding to a homogeneous mode both in plane and across the thickness, as confirmed by micromagnetic simulations (see Supplemental Material [37], which includes Refs. [38–40]). The amplitude of its resulting transmission at $P = -20$ dBm and $H_{\text{ext}} = 28$ mT is shown in Fig. 1(c). Fitting the FMR [41], we extract $\omega_0/2\pi = 2.15$ GHz, $\gamma_{\text{ext}}/2\pi = 50.06$ MHz, and $\gamma_{\text{int}}/2\pi = 8.88$ MHz for the external and internal mode damping rates, respectively.

To study nonlinear processes, we adopt a two-tone measurement scheme, as depicted in Fig. 2(a). A strong pump tone is applied with a detuning Δ from the $k = 0$ mode resonance, while a weak probe with detuning Δ_p is swept across the FMR mode spectrum to measure its response. First, we focus on the case where the pump detuning Δ is zero. As the pump power is increased above a critical value, the $k = 0$ FMR response splits into two separate resonances with equal amplitude [see Figs. 2(b) and 2(c)]. When the pump power is fixed at a value greater than the threshold and the pump detuning Δ is swept across the $k = 0$ mode, the output spectrum shows the signature of normal mode splitting [see Fig. 2(d)]. The resulting spectral line shapes also feature a small frequency distortion with power, which can be attributed to the pump not being perfectly at zero detuning, small temperature fluctuations, or a contribution from high-order nonlinearities.

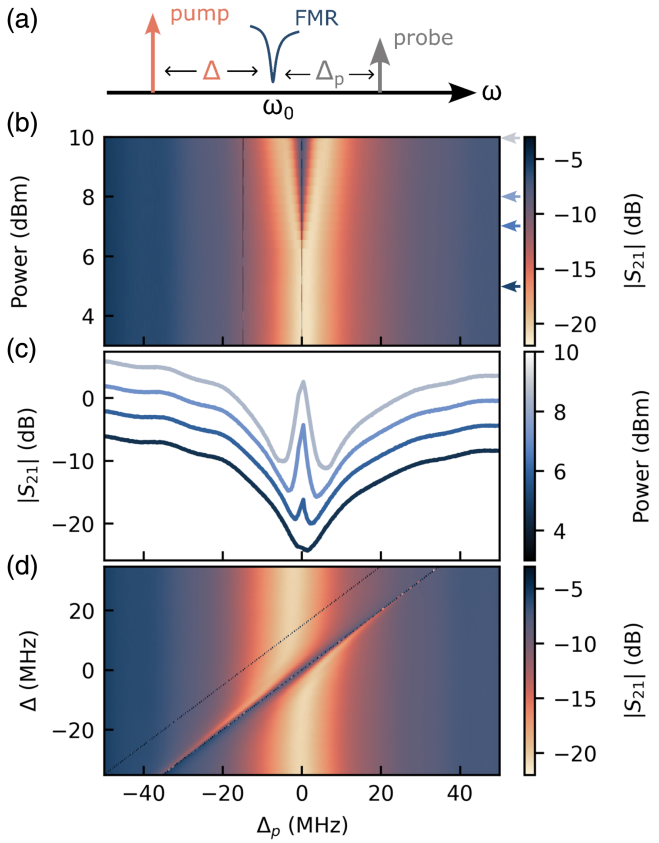

FIG. 2. FMR mode splitting of a strongly driven magnon mode at 28 mT. (a) Two-tone measurement scheme to probe three magnon processes. A strong pump is applied at detuning Δ from the FMR mode, and a small probe is swept with detuning Δ_p. (b) Map of the transmission as a function of pump power at $\Delta = 0$. (c) Line cuts extracted from (b) at the powers indicated with arrows, shifted by 4 dB for clarity, and filtered data points corresponding to the strong pump and its leak image. (d) Map of the transmission as a function of pump and probe detunings for power 10 dBm, showing normal mode splitting.

The data can be accurately represented by the microscopic theory of nonlinear spin-wave dynamics [26,28,42], achieved through the linearization of the magnon three-wave mixing process under a strong pump drive. We model our system starting from the Hamiltonian $\hat{\mathcal{H}} = \hat{\mathcal{H}}_0 + \hat{\mathcal{H}}_{\text{int}} + \hat{\mathcal{H}}_d$, in which

$$\hat{\mathcal{H}}_0/\hbar = \omega_0 \hat{m}_0^\dagger \hat{m}_0 + \sum_{k>0} \left(\omega_k \hat{m}_k^\dagger \hat{m}_k + \omega_{-k} \hat{m}_{-k}^\dagger \hat{m}_{-k}\right) \quad (1)$$

describes the bare resonant terms of the $k = 0$ mode probed by FMR, and $k \neq 0$ modes, with $\omega_k = \omega_{-k}$. The microwave drive contribution at ω_d is enclosed in the term $\hat{\mathcal{H}}_d/\hbar = i(\Omega_d^* \hat{m}_0^\dagger e^{i\omega_d t} - \Omega_d \hat{m}_0 e^{-i\omega_d t})$, where Ω_d represents the coherent amplitude (in hertz) of the driving field. The three-magnon scattering is captured by the nonlinear interaction term [24]

$$\hat{\mathcal{H}}_{\rm int}/\hbar = \sum_{k>0} V_k \hat{m}_0^\dagger \hat{m}_k \hat{m}_{-k} + \text{H.c.}, \tag{2}$$

where the coupling V_k depends on sample parameters and scales inversely proportional to the number of spins [26,28]. The magnon self-Kerr contribution and higher-order nonlinearities are not considered, as they are not necessary to explain the presented phenomenon. To find the effective interaction between the $(k, -k)$ magnon pair and the $k = 0$ mode, we further analyze the presented dynamics.

In the rotating frame at frequency ω_d, we derive the Heisenberg equations of motion for the modes and solve for the steady-state amplitudes. Under mean-field approximation, and considering $|\langle \hat{m}_k \rangle| = |\langle \hat{m}_{-k} \rangle| = \beta$, the amplitude of the coherently driven $k = 0$ mode (at $\Delta = 0$) reaches a threshold for increasing Ω_d [24,28]:

$$\langle \hat{m}_0 \rangle_{cr} = \frac{\Omega_d}{\gamma_0/2} = \frac{\gamma_k}{2V_k}, \tag{3}$$

with total loss rates γ_0 and γ_k of the $k = 0$ and down-converted modes, respectively. Since the final expression for $\langle \hat{m}_0 \rangle_{cr}$ is power independent, the number of excited magnons at $k = 0$ cannot exceed the critical value $(\gamma_k/2V_k)^2$, which is determined solely by the system parameters. Together with a saturation of the $k = 0$ mode, the $k \neq 0$ mode experiences the Suhl parametric instability and acquires a coherent amplitude, which for zero detuning is given by

$$\beta = \sqrt{\frac{4V_k\Omega_d - \gamma_0\gamma_k}{4V_k^2}}. \tag{4}$$

Equation (4) sets a lower bound on the input power strength $\Omega_{d,\rm cr} = \gamma_k\gamma_0/4V_k$ that is required for the $\omega_0/2$ mode to acquire a nonzero amplitude and an upper threshold on the saturation of the main resonant mode. This condition, which is a common trait of parametric phenomena [43,44], is due to the coherent backreaction of the magnon pair on the $k = 0$ mode once $\Omega_{d,\rm cr}$ is crossed.

The splitting feature under a strong pump emerges by linearization of the equations of motion for small fluctuations $\delta\hat{m}_{0,\pm k}$ around the steady-state solution $\hat{m}_{0,\pm k} = \langle \hat{m}_{0,\pm k} \rangle + \delta\hat{m}_{0,\pm k}$ (see Appendix B). The resulting interaction term in $\hat{\mathcal{H}}$ can be recast by performing a Bogoliubov transformation on the $\pm k$ modes. In the new basis, we introduce the modes $\hat{m}_{k+} = (i\delta\hat{m}_k + \delta\hat{m}_{-k})/\sqrt{2}$ and $\hat{m}_{k-} = (1/\sqrt{2})(\delta\hat{m}_k + i\delta\hat{m}_{-k})$, and we find that

$$\hat{\mathcal{H}}'_{\rm int}/\hbar = \sqrt{2}V_k\beta(\delta\hat{m}_0\hat{m}_{k+}^\dagger + \delta\hat{m}_0^\dagger\hat{m}_{k+}) + \hat{\mathcal{H}}_{SQ}. \tag{5}$$

Equation (5) describes a resonant beam-splitter interaction between the $k = 0$ mode and the pair of parametrically excited $\pm k$ magnon modes. The effective coupling $g_{\rm eff} = \sqrt{2}V_k\beta$ scales proportionally with the coherent amplitude of the excited magnon pair and exhibits a nonlinear dependence on the input rf pump power. The second term $\hat{\mathcal{H}}_{SQ}$ contains a single-mode squeezing contribution for mode $\hat{m}_{k+}$ and its orthogonal mode and is a consequence of the magnon three-wave mixing process. The orthogonal mode is not coupled to $\hat{m}_0$.

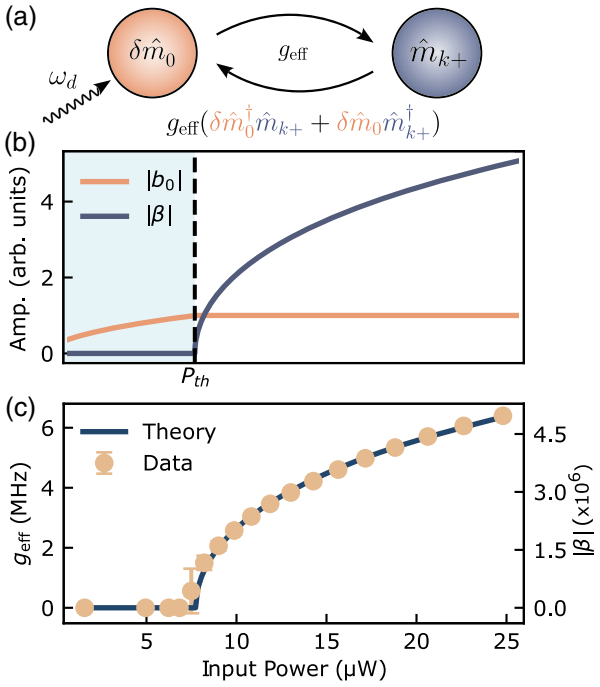

FIG. 3. Effective beam-splitter interaction between the driven $k = 0$ mode and the parametrically excited magnon pair. (a) Interaction scheme between the fluctuations of the driven $k = 0$ mode and the $\pm k$ mode. (b) Power dependence of the magnon mode amplitudes. The dashed line indicates the saturation power $P_{\rm th}$. The amplitude values are normalized to the saturation amplitude of $\hat{m}_0$. (c) Power dependence of the extracted magnon coupling $g_{\rm eff}$ from measurement data at 30 mT, fitted with Eq. (4). The right scale indicates the correspondence with the steady-state amplitude of mode β. The power scale is corrected for rf attenuation.

Figures 3(b) and 3(c) highlight the consistency between the theoretical model and experimental findings. As the pump power increases, the population of the driven mode rises until it reaches a threshold, as shown in Fig. 3(b). At this point, the amplitude of $\hat{m}_0$ saturates, and down-converted modes with $\pm k$ and amplitude $|\beta|$ are coherently excited by the strong drive. This phenomenon is evident in the experimental data, where the observed spectral splitting is proportional to $|\beta|$.

To demonstrate this proportionality, we extract the empirical effective coupling $g_{\rm eff}$ from the splitting feature in the S_{21} two-tone spectrum (see Supplemental Material [37]) and then fit the results to Eq. (4). Here, the driving rate is related to the microwave power, using standard

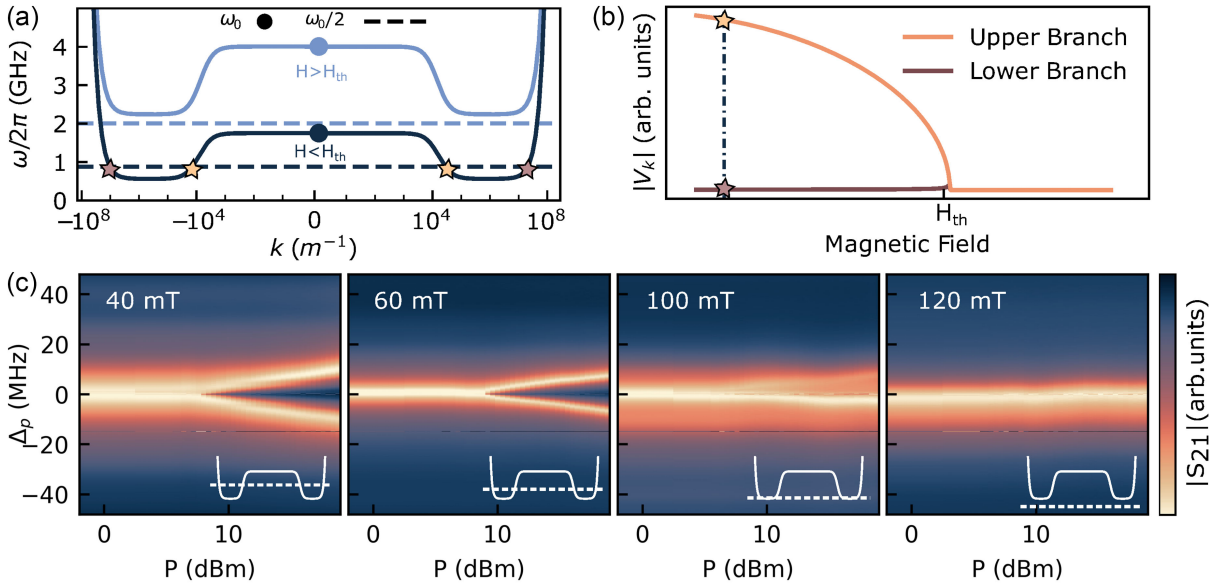

FIG. 4. Magnetic field dependence of the splitting. (a) Calculated dispersion relation for two magnetic fields below and above the threshold. Below the threshold, there are two pairs of available states at $\omega_0/2$ (dashed line), indicated with stars. (b) Calculated magnetic field dependence of the coupling V_k. The upper (lower) branch corresponds to the available state of lower (higher) k. Details of the calculation can be found in [37]. (c) Power dependence at zero pump detuning ($\Delta = 0$), for magnetic fields of 40, 60, 100, and 120 mT. In the lower right corner, a schematic illustrates the dispersion relation and the corresponding position of $\omega_0/2$.

input-output theory: $\Omega_{d,\mathrm{cr}} = \sqrt{P_{\mathrm{th}}\gamma_{\mathrm{ext}}/2\hbar\omega_0}$. The free fitting parameters are the attenuation of the rf signal in the setup and the loss term γ_k. We obtain a value of $\gamma_k = 1.77$ MHz for the $\pm k$ magnon pair mode and a total attenuation of 28 dB due to the coaxial cables and electronic instruments. Using the expression for circularly polarized waves [28], we can compute the bare three-magnon scattering strength V_k from the material parameters and external field. At 30 mT, we find a value of 0.91 Hz (see Appendix A). These calculations, illustrated in Figs. 4(a) and 4(b) and detailed in Supplemental Material [37], align well with the retrieved g_{eff}, confirming the theoretical power dependence of the down-converted mode amplitude, $|\beta|$. Similar evidence was observed in a recent Letter conducted on a YIG sphere driven at high power [45]. The arising of the splitting was interpreted via a phenomenological model.

To further support our interpretation of the observations, we study the magnetic field dependence of the measured spectral splitting. We assume that our sample has a uniform demagnetization field, which enables us to compute an approximate magnetic-field-dependent dispersion relation and coupling strength V_k, with equations shown in Appendix A. The dispersion relation of spin-waves propagating along the applied field is shown in Fig. 4(a), for two different values of the external field, above and below a threshold field H_{th}. By indicating the value of $\omega_0/2$ with a dashed line, we show that for $H < H_{\mathrm{th}}$ there are two pairs of available states marked with stars, while for $H > H_{\mathrm{th}}$ there are none. Computing V_k as a function of the field we arrive at two conclusions: (i) in the case where there are two possible pairs, the coupling of the lower k pair is 3 orders of magnitude higher, enabling us to disregard the higher k pair, and (ii) as the external field is increased, the rate diminishes until it vanishes at the point where the energy momentum conservation condition can no longer be met. These two conclusions are illustrated in Fig. 4(b), where we show V_k for the two branches with lower and higher k (upper and lower branches, respectively).

The power dependence at zero pump detuning ($\Delta = 0$) for four different magnetic fields is presented in Fig. 4(c). At 40 and 60 mT, the splitting is clear, with a slightly higher power threshold at 60 mT. At 100 mT, the splitting is barely visible, and at 120 mT, there is no splitting at all. These results yield an experimental threshold field H_{th} between 100 and 120 mT. Theoretically, an ellipsoidal sample approximation predicts $H_{\mathrm{th}} = 58$ mT [37], approximately a factor of 2 lower than the experimental value. We attribute this discrepancy to simplified assumptions in calculating the dispersion relation and V_k, particularly the neglect of inhomogeneous demagnetization fields arising from the sample's cylindrical geometry. These fields modify the dipolar dispersion and lead to other FMR modes with lower frequency than the one studied here, whose dispersion branches could also interact with the studied mode. Notably, the demonstrated magnetic field dependence of V_k provides a handle for tuning the strength of the beam-splitter interaction, enabling precise control of magnon dynamics.

In summary, we have observed the strong interaction of a magnetostatic mode with a dark mode under strong pumping, revealing a novel scheme to achieve magnon-magnon interactions. We demonstrate that the mode splitting corresponds to an excitation of a pair of magnons with

opposite momentum and half frequency. The model enables the extraction of the effective coupling, which is a direct measure of the power-dependent population of the magnon pair. It also predicts a threshold magnetic field for nonzero coupling, in agreement with experimental observations. Our results shed new light on the understanding of nonlinear parametric magnon phenomena and their dependence on bias parameters, by establishing a good agreement between theoretical predictions and experimental observations.

Recently, it was demonstrated that the higher k magnon pairs accessible through this interaction have long lifetimes of up to 18 μs at low temperatures [46]. Together with the control of the modes shown here by tuning the incident power and external bias field, it might unlock experimental routes for magnon quantum information [5,21,47].

Acknowledgments—We acknowledge V. A. S. V. Bittencourt and R. Das for helpful discussions and thank T. Bras for the help with the experimental setup. A. B.-S., H. S. J. v. d. Z., and Y. M. B. acknowledge support by the Dutch Research Council (NWO) under the project "Ronde Open Competitie XL" (File No. OCENW.XL21.XL21.058). A. B. and Y. M. B. acknowledge the support by the EU-Project No. HORIZON-EIC-2021-PATHFINDEROPEN-01 PALANTIRI-101046630. M. A. and G. A. S. acknowledge support by the Dutch Research Council (NWO) under the Project No. VI. C.212.087 of the research program VICI round 2021. C. fA. P. acknowledges the support of the Novo Nordisk Foundation, NNF Quantum Computing Programme.

M. A. proposed the experiment, performed measurements and data analysis, developed the Hamiltonian model, wrote the manuscript, and helped make the figures. A. B.-S. performed measurements and data analysis, helped with the development of the theoretical model, made the calculations for the coupling estimation and conducted Mumax3 simulations, wrote the manuscript, and made the figures. A. B. set up and postprocessed simulations on Mumax3. C. A. P. contributed to the theory development and supervised the writing. Y. M. B. supervised the theory and gave feedback on the writing. H. S. J. v. d. Z. provided the setup, gave feedback on data acquisition, helped devise the storyline, and supervised the writing process. G. A. S. contributed to the conception of the experiment, supervised the project and experimental work, came up with the explanation via three-wave mixing, helped devise the storyline, and gave feedback on the manuscript.

Data availability—The data that support the findings of this article are openly available [48].

[1] J. H. Griffiths, Anomalous high-frequency resistance of ferromagnetic metals, Nature (London) **158**, 670 (1946).
[2] C. Kittel, On the theory of ferromagnetic resonance absorption, Phys. Rev. **73**, 155 (1948).
[3] V. Kruglyak, S. Demokritov, and D. Grundler, Magnonics, J. Phys. D **43**, 264001 (2010).
[4] B. Zare Rameshti, S. Viola Kusminskiy, J. A. Haigh, K. Usami, D. Lachance-Quirion, Y. Nakamura, C.-M. Hu, H. X. Tang, G. E. Bauer, and Y. M. Blanter, Cavity magnonics, Phys. Rep. **979**, 1 (2022).
[5] H. Yuan, Y. Cao, A. Kamra, R. A. Duine, and P. Yan, Quantum magnonics: When magnon spintronics meets quantum information science, Phys. Rep. **965**, 1 (2022).
[6] P. Pirro, V. I. Vasyuchka, A. A. Serga, and B. Hillebrands, Advances in coherent magnonics, Nat. Rev. Mater. **6**, 1114 (2021).
[7] Y. Tabuchi, S. Ishino, A. Noguchi, T. Ishikawa, R. Yamazaki, K. Usami, and Y. Nakamura, Coherent coupling between a ferromagnetic magnon and a superconducting qubit, Science **349**, 405 (2015).
[8] M. Song, T. Polakovic, J. Lim, T. W. Cecil, J. Pearson, R. Divan, W.-K. Kwok, U. Welp, A. Hoffmann, K.-J. Kim *et al.*, Single-shot magnon interference in a magnon-superconducting-resonator hybrid circuit, Nat. Commun. **16**, 3649 (2025).
[9] Y. Li, W. Zhang, V. Tyberkevych, W.-K. Kwok, A. Hoffmann, and V. Novosad, Hybrid magnonics: Physics, circuits, and applications for coherent information processing, J. Appl. Phys. **128**, 130902 (2020).
[10] D. Xu, X.-K. Gu, H.-K. Li, Y.-C. Weng, Y.-P. Wang, J. Li, H. Wang, S.-Y. Zhu, and J. You, Quantum control of a single magnon in a macroscopic spin system, Phys. Rev. Lett. **130**, 193603 (2023).
[11] A. V. Chumak, A. A. Serga, and B. Hillebrands, Magnon transistor for all-magnon data processing, Nat. Commun. **5**, 4700 (2014).
[12] Ö. O. Soykal and M. Flatté, Strong field interactions between a nanomagnet and a photonic cavity, Phys. Rev. Lett. **104**, 077202 (2010).
[13] H. Huebl, C. W. Zollitsch, J. Lotze, F. Hocke, M. Greifenstein, A. Marx, R. Gross, and S. T. Goennenwein, High cooperativity in coupled microwave resonator ferrimagnetic insulator hybrids, Phys. Rev. Lett. **111**, 127003 (2013).
[14] X. Zhang, C.-L. Zou, L. Jiang, and H. X. Tang, Cavity magnomechanics, Sci. Adv. **2**, e1501286 (2016).
[15] C. A. Potts, E. Varga, V. A. S. V. Bittencourt, S. V. Kusminskiy, and J. P. Davis, Dynamical backaction magnomechanics, Phys. Rev. X **11**, 031053 (2021).
[16] S. D. Bader and S. S. P. Parkin, Spintronics, Annu. Rev. Condens. Matter Phys. **1**, 71 (2010).
[17] D. Lachance-Quirion, Y. Tabuchi, S. Ishino, A. Noguchi, T. Ishikawa, R. Yamazaki, and Y. Nakamura, Resolving quanta of collective spin excitations in a millimeter-sized ferromagnet, Sci. Adv. **3**, e1603150 (2017).
[18] Z. Rao, C. Meng, Y. Han, L. Zhu, K. Ding, and Z. An, Braiding reflectionless states in non-Hermitian magnonics, Nat. Phys. **20**, 1904 (2024).
[19] A. Kamra and W. Belzig, Super-poissonian shot noise of squeezed-magnon mediated spin transport, Phys. Rev. Lett. **116**, 146601 (2016).
[20] A. Kamra, W. Belzig, and A. Brataas, Magnon-squeezing as a niche of quantum magnonics, Appl. Phys. Lett. **117**, 090501 (2020).

[21] M. Elyasi, Y. M. Blanter, and G. E. Bauer, Resources of nonlinear cavity magnonics for quantum information, Phys. Rev. B **101**, 054402 (2020).
[22] Z. Zhang, M. O. Scully, and G. S. Agarwal, Quantum entanglement between two magnon modes via Kerr nonlinearity driven far from equilibrium, Phys. Rev. Res. **1**, 023021 (2019).
[23] P. K. Pal, A. K. Mondal, and A. Barman, Using magnons as a quantum technology platform: A perspective, J. Phys. Condens. Matter **36**, 441502 (2024).
[24] H. Suhl, The theory of ferromagnetic resonance at high signal powers, J. Phys. Chem. Solids **1**, 209 (1957).
[25] L. M. Pecora, Derivation and generalization of the Suhl spin-wave instability relations, Phys. Rev. B **37**, 5473 (1988).
[26] D. D. Stancil and A. Prabhakar, *Spin Waves* (Springer, New York, 2009).
[27] P. Krivosik and C. E. Patton, Hamiltonian formulation of nonlinear spin-wave dynamics: Theory and applications, Phys. Rev. B **82**, 184428 (2010).
[28] V. S. L'vov, *Wave Turbulence Under Parametric Excitation: Applications to Magnets* (Springer Science & Business Media, New York, 2012).
[29] E. Schlömann, J. Green, and U. Milano, Recent developments in ferromagnetic resonance at high power levels, J. Appl. Phys. **31**, S386 (1960).
[30] O. Lee, K. Yamamoto, M. Umeda, C. W. Zollitsch, M. Elyasi, T. Kikkawa, E. Saitoh, G. E. Bauer, and H. Kurebayashi, Nonlinear magnon polaritons, Phys. Rev. Lett. **130**, 046703 (2023).
[31] I. Barsukov, H. Lee, A. Jara, Y.-J. Chen, A. Gonçalves, C. Sha, J. Katine, R. Arias, B. Ivanov, and I. Krivorotov, Giant nonlinear damping in nanoscale ferromagnets, Sci. Adv. **5**, eaav6943 (2019).
[32] L. Sheng, M. Elyasi, J. Chen, W. He, Y. Wang, H. Wang, H. Feng, Y. Zhang, I. Medlej, S. Liu *et al.*, Nonlocal detection of interlayer three-magnon coupling, Phys. Rev. Lett. **130**, 046701 (2023).
[33] L. Körber, K. Schultheiss, T. Hula, R. Verba, J. Fassbender, A. Kákay, and H. Schultheiss, Nonlocal stimulation of three-magnon splitting in a magnetic vortex, Phys. Rev. Lett. **125**, 207203 (2020).
[34] S. Kimura and I. Shindo, Single crystal growth of yig by the floating zone method, J. Cryst. Growth **41**, 192 (1977).
[35] M. Sparks, Ferromagnetic resonance in thin films. I. Theory of normal-mode frequencies, Phys. Rev. B **1**, 3831 (1970).
[36] E. R. Edwards, M. Buchmeier, V. E. Demidov, and S. O. Demokritov, Magnetostatic spin-wave modes of an in-plane magnetized garnet-film disk, J. Appl. Phys. **113**, 103901 (2013).
[37] See Supplemental Material at http://link.aps.org/supplemental/10.1103/jnpb-2mxx for information on measurement setup, additional measurement data, data analysis routine and theoretical modelling.
[38] A. Vansteenkiste, J. Leliaert, M. Dvornik, M. Helsen, F. Garcia-Sanchez, and B. Van Waeyenberge, The design and verification of Mumax3, AIP Adv. **4**, 107133 (2014).
[39] L. Exl, S. Bance, F. Reichel, T. Schrefl, H. Peter Stimming, and N. J. Mauser, Labonte's method revisited: An effective steepest descent method for micromagnetic energy minimization, J. Appl. Phys. **115**, 17D118 (2014).
[40] M. F. Gely, A. Sanz Mora, S. Yanai, R. Van der Spek, D. Bothner, and G. A. Steele, Apparent nonlinear damping triggered by quantum fluctuations, Nat. Commun. **14**, 7566 (2023).
[41] S. Probst, F. Song, P. A. Bushev, A. V. Ustinov, and M. Weides, Efficient and robust analysis of complex scattering data under noise in microwave resonators, Rev. Sci. Instrum. **86**, 024706 (2015).
[42] H. Suhl and X. Zhang, Spin-wave instabilities and their revival by nonlinear mechanics, J. Appl. Phys. **63**, 4147 (1988).
[43] K. Hill, D. Johnson, B. Kawasaki, and R. MacDonald, Cw three-wave mixing in single-mode optical fibers, J. Appl. Phys. **49**, 5098 (1978).
[44] A. Zorin, Josephson traveling-wave parametric amplifier with three-wave mixing, Phys. Rev. Appl. **6**, 034006 (2016).
[45] J. Rao, B. Yao, C. Wang, C. Zhang, T. Yu, and W. Lu, Unveiling a pump-induced magnon mode via its strong interaction with Walker modes, Phys. Rev. Lett. **130**, 046705 (2023).
[46] R. O. Serha, K. H. McAllister, F. Majcen, S. Knauer, T. Reimann, C. Dubs, G. A. Melkov, A. A. Serga, V. S. Tyberkevych, A. V. Chumak, and D. A. Bozhko, Ultra-long-living magnons in the quantum limit, arXiv:2505.22773.
[47] K. An, M. Xu, A. Mucchietto, C. Kim, K.-W. Moon, C. Hwang, and D. Grundler, Emergent coherent modes in nonlinear magnonic waveguides detected at ultra-high frequency resolution, Nat. Commun. **15**, 7302 (2024).
[48] Data available at Zenodo, 10.5281/zenodo.16876694.

End Matter

Appendix A: Dispersion relation and three magnon scattering coupling strength—Understanding the dispersion relation in the sample is crucial to identifying the magnon ($\hat{m}_k$) modes available for three-wave mixing that satisfy energy and momentum conservation. Analytical expressions for the dispersion relation of an in-plane magnetized thin disk have not been comprehensively addressed in the literature. Sparks [35] described dispersion relations for out-of-plane magnetized disks and some specific modes in in-plane magnetized configurations. The primary challenge lies in solving the Walker equations to accurately determine the sample's demagnetization field. However, given the large radius and thickness of our sample, the dispersion relation can be approximated by that of an ellipsoid as a reasonable first-order approximation. Using a frame of reference with z in the out-of-plane direction and the feedline and magnetic field aligned along x, we can define [28]

$$A_k = \mu_0\gamma\left(H + M_S\lambda_{ex}k^2 + M_S\frac{k_y^2+k_z^2}{2k^2}\right),$$
$$B_k = \mu_0\gamma M_S\frac{(k_y+ik_z)^2}{2k^2}, \tag{A1}$$

such that

$$\omega_k = \sqrt{A_k^2 - |B_k|^2}. \tag{A2}$$

Here, μ_0 is the permeability of free space, γ the gyromagnetic ratio, H the external magnetic field, M_S the saturation magnetization, and λ_{ex} the exchange stiffness constant and k the modulus of the momentum $\left(k = \sqrt{k_x^2+k_y^2+k_z^2}\right)$. This gives the dispersion for a homogeneous mode and completely disregards all other magnetostatic modes mentioned earlier and shown in Supplemental Material [37].

To have available states for three-wave mixing, it is required to have a dispersion that has lower frequencies for increasing k in some range of the dispersion. That happens for any branch other than the Damon-Eshbach branch ($k_x = 0$) and is most pronounced for $k_y = 0$, that is, for backward volume magnetostatic waves.

The coupling of a magnetostatic mode to a pair of such k states was calculated for ellipsoidal samples with homogeneous demagnetization in [28] and is given by

$$V_k = \omega_M\sqrt{\frac{g_{\mathrm{eff}}\mu_B}{2\nu M_S}}\left(1+\frac{\omega_k}{A_k+|B_k|}\right)\frac{k_x(k_y+ik_z)}{k^2}, \tag{A3}$$

where $\omega_M = \mu_0\gamma M_S$. The first insight this equation provides is that for pure backward volume spin-waves—i.e., k is parallel to the magnetization, $k_y = k_z = 0$—the coupling is zero. The situation for which one finds the higher coupling is for $k_y = 0$, and $k_z = \pi/t$, corresponding to one node along the thickness direction. With these values, taking an external field of 30 mT and the material parameters, we found $V_k = 0.91$ Hz. This result does not provide accurate values of the coupling rate in our geometry, due to the mismatch in the considered demagnetization field. Still, it enables us to get an order-of-magnitude estimate of the coupling and evaluate which of the two pairs of magnons that are enabled by E-k conservation participate more strongly in the process.

These calculations provide only order-of-magnitude estimates of the coupling and understanding of the participating modes. To get a better estimate, even within the ellipsoidal sample approximation, one would need to consider all k modes for which the E-k condition is satisfied. Those will be a continuum along k_y and a sum of discrete modes with $k_z = n\pi/t$. The next step toward a more quantitative theory would be to include the nonuniform demagnetization field and the rest of the magnetostatic modes. Those modes have a corresponding dispersion relation to which the uniform mode could couple, influencing the coupling rate and the magnetic field threshold.

Appendix B: Three-wave mixing hamiltonian and linearized dynamics—We present here the key steps connecting three-magnon scattering with the emergence of an effective magnon-magnon beam-splitter interaction. The complete derivation and dynamics can be found in Supplemental Material [37]. We start from the Hamiltonian $\hat{\mathcal{H}}_0$ of a quasimagnetostatic mode $\hat{m}_0$ coupled via a three-wave mixing interaction $\hat{\mathcal{H}}_{\mathrm{int}}$ to a pair of counter-propagating modes $\hat{m}_{\pm k}$ with momentum $|k| \neq 0$ living in the spin-wave continuum, where

$$\hat{\mathcal{H}}_0/\hbar = \omega_0\hat{m}_0^\dagger\hat{m}_0 + \sum_{k>0}\left(\omega_k\hat{m}_k^\dagger\hat{m}_k + \omega_{-k}\hat{m}_{-k}^\dagger\hat{m}_{-k}\right) \tag{B1}$$

and

$$\hat{\mathcal{H}}_{\mathrm{int}}/\hbar = \sum_{k>0}V_k\hat{m}_0^\dagger\hat{m}_k\hat{m}_{-k} + \mathrm{H.c.} \tag{B2}$$

Here, ω_0 and $\omega_k = \omega_{-k}$ represent the frequencies of the $k = 0$ and $|k| \neq 0$ magnon modes, respectively, while V_k characterizes the strength of the bare three-magnon process. The FMR mode is coherently excited by a microwave drive at ω_d of the form $\hat{\mathcal{H}}_d/\hbar = i(\Omega_d^*\hat{m}_0^\dagger e^{i\omega_d t} - \Omega_d\hat{m}_0 e^{-i\omega_d t})$, where Ω_d describes the amplitude (in hertz) of the driving field. To fully remove the time dependence from the Hamiltonian, we can apply in sequence two unitary operations. The first, $\hat{U}(t) = e^{i\omega_d\hat{m}_0^\dagger\hat{m}_0 t}$ allows us to move to a frame rotating at the drive frequency ω_d, followed by the transformation $\hat{U}(t) = e^{i\omega_d/2\hat{m}_k^\dagger\hat{m}_k t}e^{i\omega_d/2\hat{m}_{-k}^\dagger\hat{m}_{-k}t}$ to a frame corotating at the frequency of the $\hat{m}_{\pm k}$ modes. By retaining the coupling to a single pair of $\pm k$ modes, we can rewrite the resulting Hamiltonian as

$$\begin{aligned}\hat{\mathcal{H}}/\hbar = {}& \Delta_0\hat{m}_0^\dagger\hat{m}_0 + \Delta_k\hat{m}_k^\dagger\hat{m}_k + \Delta_{-k}\hat{m}_{-k}^\dagger\hat{m}_{-k} \\ & + V_k^*\hat{m}_0\hat{m}_k^\dagger\hat{m}_{-k}^\dagger + V_k\hat{m}_0^\dagger\hat{m}_k\hat{m}_{-k} \\ & + i(\Omega_d^*\hat{m}_0 - \Omega_d\hat{m}_0^\dagger),\end{aligned} \tag{B3}$$

where we have introduced the detuning with respect to the drive $\Delta_0 = \omega_0 - \omega_d$ and the mode detuning $\Delta_{\pm k} = \omega_{\pm k} - \omega_0/2$. After the derivation of the steady-state solution amplitudes [37], for large input drive powers we can focus on the dynamics of the fluctuations around these solutions $\hat{\mathcal{O}} = \langle\hat{\mathcal{O}}\rangle + \delta\hat{\mathcal{O}}$. Following the argument in Supplemental Material [37], we can assume V_k and $\langle\hat{m}_k\rangle = \beta$ to be real and by the gauge of choice that $\langle\hat{m}_{-k}\rangle = i\beta$. If we expand the three-wave mixing

interaction term around the steady state

$$\hat{m}_0\hat{m}_k^\dagger\hat{m}_{-k}^\dagger \to (\langle\hat{m}_0\rangle + \delta\hat{m}_0)(\beta + \delta\hat{m}_k^\dagger)(-i\beta + \delta\hat{m}_{-k}^\dagger) \quad \text{(B4)}$$

and keep only terms quadratic in the fluctuations, we arrive at

$$\hat{m}_0\hat{m}_k^\dagger\hat{m}_{-k}^\dagger \to \langle\hat{m}_0\rangle\delta\hat{m}_k^\dagger\delta\hat{m}_{-k}^\dagger + \beta\delta\hat{m}_0\delta\hat{m}_{-k}^\dagger - i\beta\delta\hat{m}_0\delta\hat{m}_k^\dagger. \quad \text{(B5)}$$

From here, the Hamiltonian can be recast in a simpler form by performing a Bogoliubov transformation to a collective mode basis defined by

$$\hat{m}_{k+} = \frac{1}{\sqrt{2}}(i\delta\hat{m}_k + \delta\hat{m}_{-k}), \quad \text{(B6)}$$

$$\hat{m}_{k-} = \frac{1}{\sqrt{2}}(\delta\hat{m}_k + i\delta\hat{m}_{-k}), \quad \text{(B7)}$$

which enables one to redefine the original modes as

$$\delta\hat{m}_k = \frac{1}{\sqrt{2}}(-i\hat{m}_{k+} + \hat{m}_{k-}), \quad \text{(B8)}$$

$$\delta\hat{m}_{-k} = \frac{1}{\sqrt{2}}(\hat{m}_{k+} - i\hat{m}_{k-}). \quad \text{(B9)}$$

As a consequence, in the new canonical basis, the interaction Hamiltonian takes the form

$$\hat{\mathcal{H}}'_{\rm int}/\hbar = \sqrt{2}V_k\beta(\delta\hat{m}_0\hat{m}_{k+}^\dagger + \delta\hat{m}_0^\dagger\hat{m}_{k+}) + H_{SQ}. \quad \text{(B10)}$$

In the linearized dynamics, the first term describes a power-dependent effective beam-splitter interaction between the driven $k = 0$ mode and the collective pair excitation at $\pm k$. The second term, given by

$$H_{SQ} = -\frac{iV_k}{2}\langle m_0\rangle\left[(\hat{m}_{k+})^2 - (\hat{m}_{k+}^\dagger)^2 + (\hat{m}_{k-})^2 - (\hat{m}_{k-}^\dagger)^2\right], \quad \text{(B11)}$$

refers to a single-mode squeezing interaction for the counterpropagating modes whose strength is limited by the occupation of the FMR mode amplitude.